frontiers | Frontiers in Marine Science

TYPE Original Research
PUBLISHED 08 January 2024
DOI 10.3389/fmars.2023.1284750

OPEN ACCESS

EDITED BY
Zhifang Xiong,
Ministry of Natural Resources, China

REVIEWED BY
Grant Bigg,
The University of Sheffield, United Kingdom
Thomas Algeo,
University of Cincinnati, United States

*CORRESPONDENCE
Qian Ge
qge@sio.org.cn

RECEIVED 30 August 2023
ACCEPTED 15 December 2023
PUBLISHED 08 January 2024

CITATION
Lei Z, Ge Q, Chen D, Zhang Y and Han X (2024) Impact of circumpolar deep water on organic carbon isotopes and ice-rafted debris in West Antarctic: a case study in the Amundsen Sea.
Front. Mar. Sci. 10:1284750.
doi: 10.3389/fmars.2023.1284750

Impact of circumpolar deep water on organic carbon isotopes and ice-rafted debris in West Antarctic: a case study in the Amundsen Sea

Ziyan Lei[1,2,3], Qian Ge[1,2]*, Dong Chen[1,2], Yongcong Zhang[1,2] and Xibin Han[1,2]

[1]Key Laboratory of Submarine Geosciences, Ministry of Natural Resources, Hangzhou, China, [2]Second Institute of Oceanography, Ministry of Natural Resources, Hangzhou, China, [3]Department of Oceanography and Coastal Science, Louisiana State University, Baton Rouge, LA, United States

This research delves into the interaction between carbon isotopes, ice-rafted debris (IRD), and Circumpolar Deep Water (CDW) in the Amundsen Sea, West Antarctic. Utilizing sediment core ANT36-A11-04, we traced the source of the organic matter though an analysis of the total organic carbon (TOC), stable carbon isotopes ($\delta^{13}C_{org}$), and nitrogen content. We identified six environmental events in this region since the Mid-Holocene, which were discerned through a comparative analysis of the $\delta^{13}C_{org}$, TOC, and IRD content. These events were closely linked to variations in the intensity of the CDW. Notably, the synchronous occurrence of a negative shift in the $\delta^{13}C_{org}$ value and increases in TOC and IRD highlight the significant impact of CDW intrusion, underlining the pivotal role of the CDW in the regional environmental evolution. Specifically, intensified upwelling of the CDW was correlated with increased heat and nutrients, enhanced glacier melting, phytoplankton blooms, higher TOC content, augmented deposition of IRD, and finally resulted in a negative shift in the $\delta^{13}C_{org}$ value. We present a comprehensive picture of the local environmental evolution in the Amundsen Sea, characterized as a marine-glacial-biological coupling model, thereby contributing to a broader understanding of Antarctic environmental dynamics.

KEYWORDS

paleoenvironment, evolution pattern, organic matter, geochemistry, sediment

Highlights

- The organic matter source of the sediments in Core ANT36-A11-04 was analyzed.
- The 6000-yr paleoenvironmental evolution was reconstructed via indicators.
- Six events were identified via indexes and corresponding records.
- Circumpolar Deep Water plays a key role in environmental evolution.

1 Introduction

The Antarctic environment is experiencing significant transformations. Recent satellite data reveal that over the last two decades, the West Antarctic Ice Sheet (WAIS) has been diminishing at an alarming rate of 100–200 Gt per year. This decline contributes to a rise in sea level of approximately 0.25–0.26 mm per year (Joughin and Alley, 2011). Notably, the Amundsen Sea region exhibits pronounced changes, with the Pine Island and Thwaites ice shelves experiencing the most substantial mass losses. These shelves, as floating extensions of the ice sheet, play a crucial role in buttressing the ice sheet. Their melting leads to accelerated flow of the upstream glaciers into the ocean, significantly impacting global sea levels (Gudmundsson et al., 2019; Naughten et al., 2023). The vulnerability of the WAIS to warm, moist oceanic air and sub-shelf currents is a key factor driving these changes (Jenkins et al., 2010; Nicolas and Bromwich, 2011). In the Amundsen Sea, the melting of the ice shelf is predominantly influenced by the upwelling of the Circumpolar Deep Water (CDW). This warmer water not only transports heat and nutrients but also plays a vital role in shaping the regional sea ice dynamics and ecosystems (Nakayama et al., 2014; Nakayama et al., 2018; van Manen et al., 2022).

Research on the CDW in the Amundsen Sea has predominantly concentrated on modeling the intrusion of the CDW and examining variations in the temperature and salinity within the water column (Thoma et al., 2008; Nakayama et al., 2013; Mallett et al., 2018). However, there is a notable gap in research on the historical evolution of the CDW and its correlations with various indicators in sediment and ice-rafted debris (IRD). We aim to shed light on the paleoenvironmental shifts in the Amundsen Sea and to investigate how organic components and IRD respond to the influence of the CDW. This approach enables us to unravel the underlying mechanisms driving environmental changes in this region.

2 Materials and methods

Sediment samples were collected from push core ANT36-A11-04, which was obtained during the 36th Chinese National Antarctic Research Expedition (2019–2020). The sampling site, situated at a depth of 500 meters in the Amundsen Sea, West Antarctic (117.835° W, 72.028°S) is depicted in Figure 1. Following the collection, these samples were meticulously preserved at 4°C in a freezer, pending analysis. The processing in the laboratory adhered strictly to the

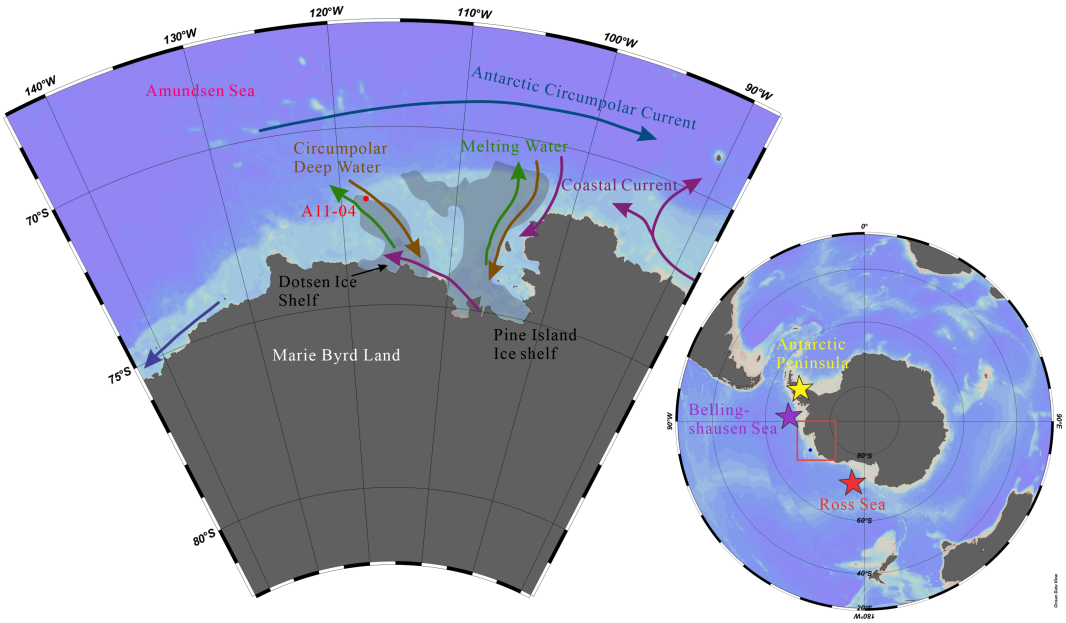

FIGURE 1
Map of the currents and station. The map on the right side is an overall map of the Antarctic. The red rectangle is the study area in the Amundsen Sea, the yellow star denotes Antarctic Peninsula, the purple star denotes the Bellingshausen Sea, and the red star denotes the Ross Sea. The map on the left side is a detailed map of the study area. The arrows represent the currents. The purple arrow is the costal current, green arrow is melting water, the brown arrow is the Circumpolar Deep Water, and the deep blue arrow is the Antarctic Circumpolar Current. The two grey shaded areas are the two biggest ice shelves in this region.

Specifications for oceanographic survey - Part 8: marine geology and geophysics survey (Liu et al., 2007). The core was 38 cm long and characterized by a dark grayish-brown hue. It was sectioned at 1-cm intervals, resulting in the attainment and analysis of 36 distinct samples.

Antarctica shelf sediments typically lack calcareous foraminifera, which are commonly used in radiocarbon dating due to their well-established reservoir adjustments (Smith et al., 2014). Consequently, dating the acid insoluble organic (AIO) fraction becomes necessary. However, bulk AIO dates often face contamination risks from ancient organic matter eroded from the Antarctica continent (Licht et al., 1996; Anderson and Andrews et al., 1999; Ohkouchi and Eglinton, 2006) or the redistribution of older shelf sediments (Domack et al., 1999), potentially leading to anomalously older radiocarbon ages. Despite these challenges, several studies have effectively employed AIO fraction dates to establish deglacial chronologies for the Antarctica shelf (Domack et al., 1999; Licht and Andrews, 2002; Mosola and Anderson, 2006; Heroy and Anderson, 2007; Hillenbrand et al., 2010; Smith et al., 2011; Licht and Hemming, 2017).

For core ANT36-A11-04, we implemented a rigorous dating methodology, integrating sedimentological and geochemical data to identify optimal horizons for accurate ^{14}C dating. Notable shifts in these data, potentially indicative of significant environmental changes (Figure 2), guided the selection of six samples for accelerator mass spectrometry (AMS) ^{14}C dating at Beta Laboratories, USA (Table 1), complemented by ^{210}Pb dating methods (Figure 3). Age corrections were made using the Calib 8.2 program (Stuiver and Reimer, 1993). It was assumed that the regional marine offset (ΔR) was 900 ± 100, which is consistent with the global marine reservoir effect and previous studies conducted in the Amundsen Sea Embayment (Lowe and Anderson, 2002; Hillenbrand et al., 2010).

Grain size analysis was conducted using a Malvern 2000 laser particle size analyzer at the Second Institute of Oceanography, Ministry of Natural Resources, Hangzhou, Zhejiang Province, China, following the Specifications for oceanographic survey - Part 8: marine geology and geophysics survey (Liu et al., 2007).

The organic carbon and nitrogen contents and isotope compositions were also analyzed at the Second Institute of Oceanography. Freeze-dried samples were milled to a size of less than 120 μm. Excess 1 M hydrochloric acid was added to the samples, which were then left to react for 24 hours to remove the carbonate. After neutralizing the samples with deionized water, the samples were lyophilized. For the $\delta^{13}C_{org}$ and organic carbon content analyses, 1–4 mg of the treated samples were wrapped in tin cups, while the nitrogen content analysis required a ten-fold increase in the sample weight. Isotope ratio mass spectrometry (Thermo Delta Plus AD, Germany) was used to conduct the $\delta^{13}C_{org}$ analysis of the sediments, and the results were calibrated against standards USGS-24, GBW4407, and IAEA-N-1. The $\delta^{13}C_{org}$ data have an accuracy of ±0.2‰ in reference to the Pee Dee Belemnite (PDB) international standard. The organic carbon and nitrogen contents were analyzed using an Elementar Vario (Germany), with an analytical accuracy of ±0.01%.

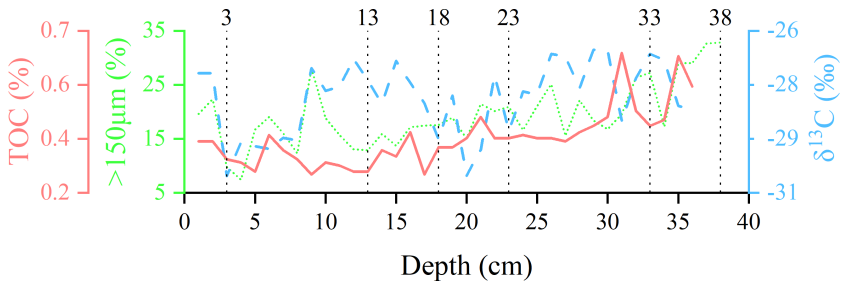

FIGURE 2
Comparison of grain size and geochemistry for the sediments in core ANT36-A11-04. The red solid line denotes the total organic carbon (TOC), the green dot line denotes the > 150 μm particle content, and the blue dash line denotes the $\delta^{13}C_{org}$.

TABLE 1 Dating results and sedimentation rate for sediment in core ANT36-A11-04 or financial relationships that could be construed as a potential conflict of interest.

Depth (cm)	AMS ^{14}C (cal yr B.P.)	Calibrated Age (a)	Old Carbonate Age (a)	Calendar Age (cal yr B.P)	Sedimentation rate (cm/kyr)
2–3	5100 ± 30	4096	4096	0	6.66
12–13	6730 ± 30	6047	4096	1951	
17–18	8310 ± 30	7693	4096	3597	3.04
22–23	9450 ± 30	8979	4096	4883	3.04
32–33	10230 ± 50	9951	4096	5855	10.29
37–38	10400 ± 30	10245	4096	6149	17.01

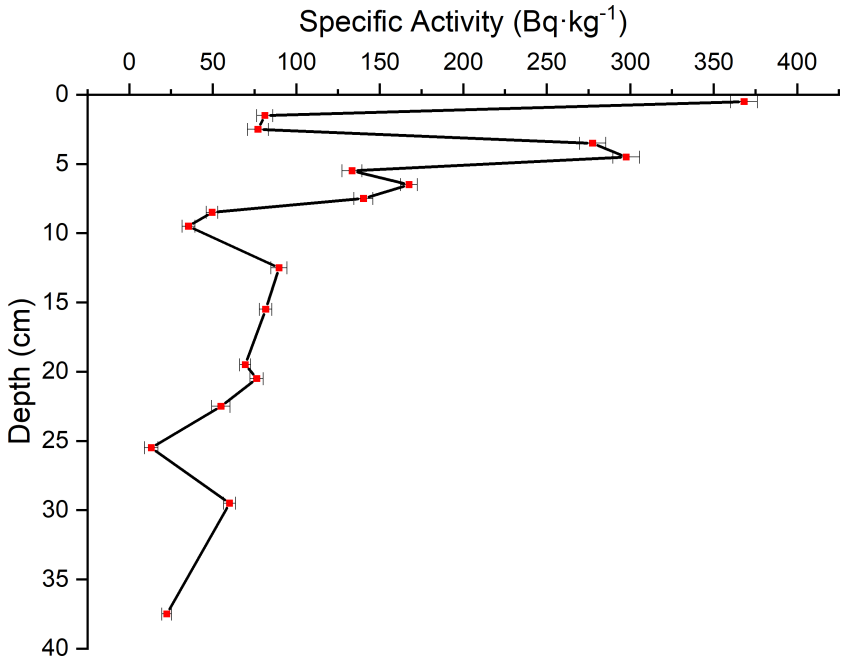

FIGURE 3
$^{210}Pb_{ex}$ profile of sediment in core ANT36-A11-04.

3 Results

3.1 Chronology

Figure 3 shows that there is a distinct exponential decrease in the excess 210Pb activity from the surface to a depth of 10 cm in the sediment from core ANT36-A11-04. It stabilizes at background levels below this depth. This trend suggests that the uppermost layer is indicative of recent sedimentation. Via age calibration using the Calib 8.2 software, we estimate that the calendar age of the sediment at depths of 2–3 cm is approximately 4096 years before present (B.P.). In light of the 210Pb activity profile, this age is interpreted as the old carbon age for this region. As a result, all of the AMS ^{14}C dating results were corrected by subtracting the age of the top of the core (4096 cal yr B.P.) Through linear interpolation and extrapolation of these corrected ages, we estimate that the calendar age at the base of the sediment is 6149 cal yr B.P. The sedimentation rates (Table 1) range from 3.0 cm/kyr to 17.0 cm/kyr. The limited quantity of sediment in the lowermost layers (36 cm to 38 cm) precluded the acquisition of data on the organic carbon, nitrogen, and carbon isotopes, but grain size analysis was conducted. Consequently, in the subsequent analyses, the age of the 35-cm layer, approximately 6031 cal yr B.P., is uniformly adopted as the representative age of the bottom layer.

3.2 Organic carbon content, nitrogen content, and organic carbon isotopes

In core ANT36-A11-04, the total organic carbon (TOC) content varied notably, ranging from 0.26% to 0.66%, with an average of 0.38% (Figure 4). The TOC content peaked between 6000 and 5200 cal yr B.P., reached the highest level, and subsequently remained a lower range of 0.26–0.45% after 5200 cal yr B.P. Regarding the total nitrogen (TN) content, it oscillated between 0.02% to 0.06%. A distinct shift occurred around 4000 cal yr B.P., that is, from 6000 to 4000 cal yr B.P., the TN content varied between 0.04% and 0.06%, with an average of 0.05%. After 4000 cal yr B.P., it ranged from 0.02% to 0.04%, with an average of 0.03%. The carbon to nitrogen ratio (C/N) also fluctuated, ranging from 6.6 to 17.9, with an overall average of 10.78. The $\delta^{13}C_{org}$ value underwent significant variation, ranging from –30.75‰ to –26.33‰, with an average of –28.07‰. The lowest and highest $\delta^{13}C_{org}$ values occurred at 177 cal yr B.P. and 5369 cal yr B.P., respectively.

3.3 Grain size

Figure 5 depicts the changes in the grain size and compositional characteristics of the sediments in core ANT36-A11-04. The sediment composition varied. Silt was predominant (average of 41.2%), followed by sand (38.7%) and clay (19.9%). The grain size composition characteristics can be categorized into two distinct stages. From 3600 cal yr B.P. onwards, the mean grain size (Mz), skewness, kurtosis, and sand content generally remained below the average values, with a notable exception around 1500 cal yr B.P. when they exceeded the average values. Conversely, during this stage, the silt and clay contents exhibited inverse trends. The sorting coefficient, skewness, and kurtosis exhibited minimal variation, suggesting a more uniform grain size distribution. In contrast, from 6149 to 3600 cal yr B.P, the Mz, skewness, kurtosis, and sand content consistently exceeded the average values, while the silt and clay contents were lower. During this period, the average skewness was 0.56, indicative of right-skewness, and the average kurtosis was 2.32.

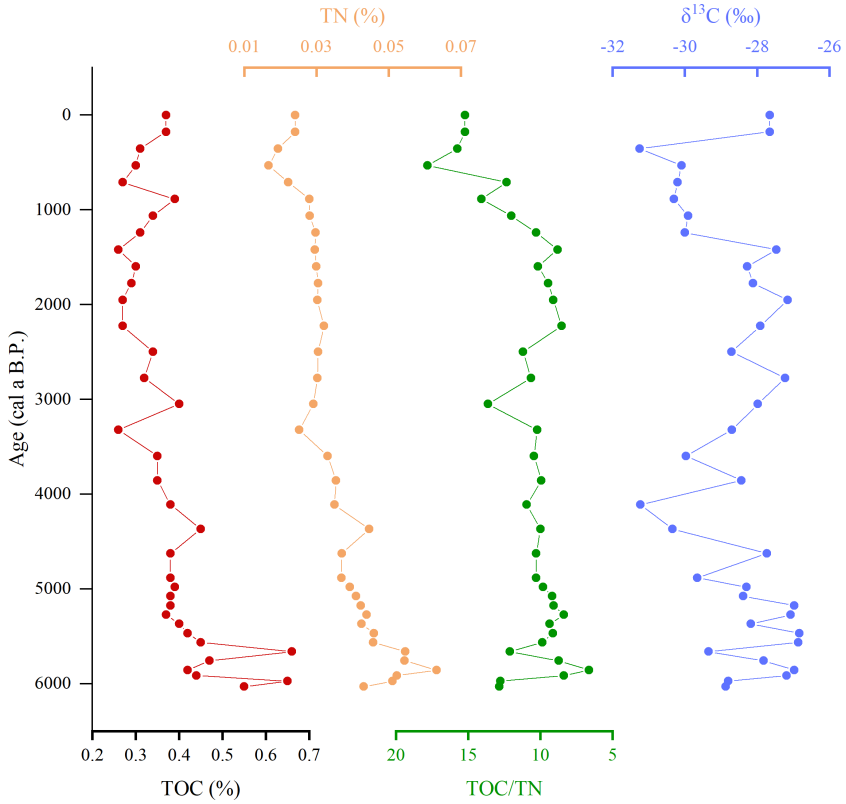

FIGURE 4
Vertical variations in TOC, TN, C/N, and $\delta^{13}C$ for the sediments in core ANT36-A11-04.

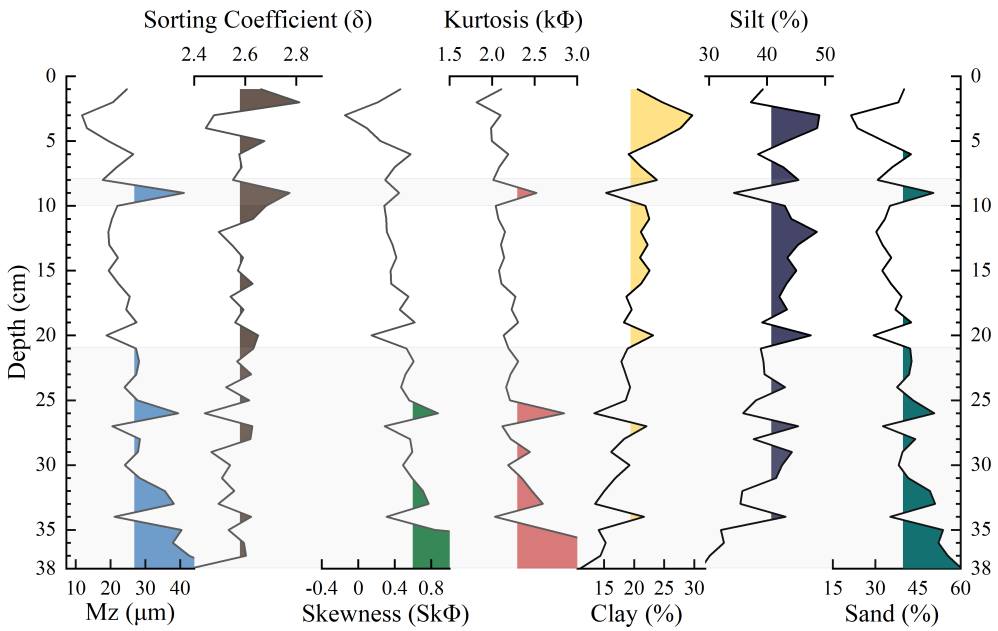

FIGURE 5
Grain size characteristics of sediments in core ANT36-A11-04. The colorful shaded area represents that this layer is beyond the average value. The grey shaded area denotes that the data within these depths are distinct from the data for the other depths.

This earlier phase was characterized by higher levels of skewness, kurtosis, and sand-grade components, implying that the provenance of the sand-grade components was distinct from that in the later stage.

4 Discussion

4.1 TOC and $\delta^{13}C_{org}$ profiles: indicators of paleoenvironmental conditions

The Antarctic environment imparts distinct characteristics to the stable carbon isotope compositions of marine organic materials, markedly differing from those at lower latitudes. The notably low (depleted) $\delta^{13}C_{org}$ values of Antarctic plankton have been attributed to several factors: the low water temperature and resultant high CO_2 availability (Rau et al., 1989), the specific species composition of the plankton, and the upwelling of deep water (Lupton and Craig, 1981; Spezie, 1999). In Antarctic waters, the surface-water CO_2 concentrations can be up to 2.5 times higher than those in equatorial waters, primarily due to the lower temperatures. This increase in the CO_2 concentration, coupled with the temperature decrease, likely contributes to the reduction in the $\delta^{13}C_{org}$ values at higher latitudes. Additionally, the upwelling of deep waters, which are enriched in dissolved CO_2 with low $\delta^{13}C$ values due to the remineralization of organic matter, further influences this biological processing in the surface water. Consequently, $\delta^{13}C_{org}$ is a potential indicator of environmental change and is a focal point in this study.

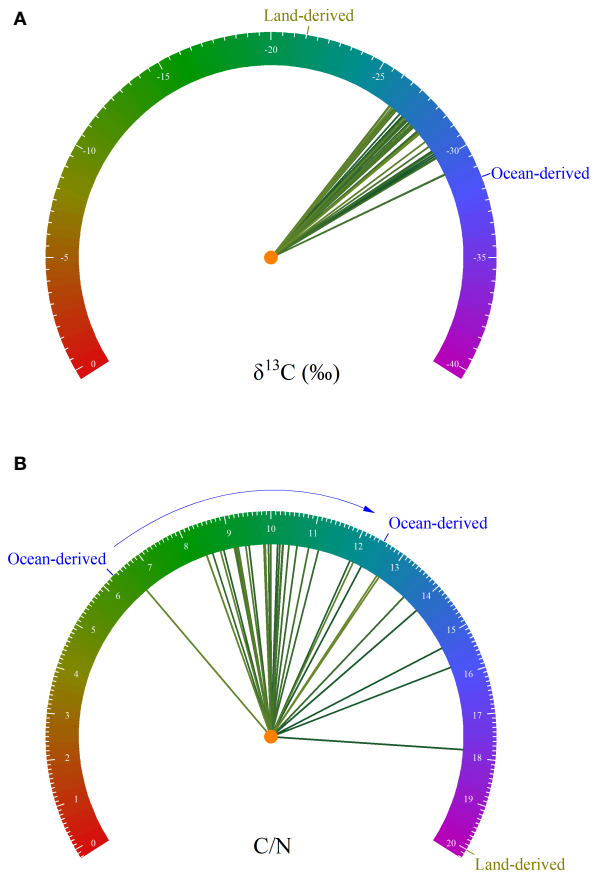

FIGURE 6
Organic matter source discriminant diagram for core ANT36-A11-04. **(A)** $\delta^{13}C_{org}$ value and endmember value of the sediments in core ANT36-A11-04 (Shultz and Calder, 1976; Minoura et al., 1997). The region delineated by the blue arrow, marking the range of 6.3 to 12.4, suggests a marine origin for the organic matter. A C/N ratio of greater than 20 indicates that the organic matter has a terrestrial origin. **(B)** C/N value and end-member value of the organic matter in ANT36-A11-04 (Albuquerque and Mozeto, 1997; Stein and Fahl, 2000). The values close to the blue area signify a marine source for the organic matter, while proximity to the green area indicates a terrestrial source.

The study area is predominantly influenced by the colonial haptophyte *Phaeocystis antarctica*, known for its specific organic carbon isotope ratio ($\delta^{13}C_{org}$). This ratio typically ranges between –28.34‰ and –29.86‰ (Delmont et al., 2014; Ducklow et al., 2015), which is very consistent with our data (i.e., –30.75‰ to –26.33‰, average of –28.07‰). These findings suggest that marine phytoplankton made a significant contribution to the organic carbon in the sediment in core ANT36-A11-04. To ascertain the organic carbon source, we used a $\delta^{13}C_{org}$ value of –31.5‰ for West Antarctic phytoplankton as the marine endmember, and a value of –23.6‰ for East Antarctic terrestrial mosses, lichens, and freshwater lake algae as the terrestrial endmember (Shultz and Calder, 1976; Minoura et al., 1997). Our analysis revealed that the organic carbon in the core predominantly originated from marine sources (Figure 6). Furthermore, due to the fact that terrestrial plants are composed of nitrogen-poor lignin and cellulose, while marine organisms are contain nitrogen-rich proteins marine and terrestrial sources of organic matter have distinct C/N values. Terrestrial plants typically have C/N values of > 20 (Albuquerque and Mozeto, 1997), whereas that of high-latitude marine phytoplankton ranges from 6.3 to 12.5 (Stein and Fahl, 2000). As depicted in Figure 6, C/N values of > 20 suggest a terrestrial plant origin, while values of 6.3–12.5 indicate a contribution from marine phytoplankton. The average C/N value of 10.8 for the core suggests a primarily marine phytoplankton source. However, the variation in the C/N values from 6.6 to 17.8 implies possible terrestrial inputs or the influences of early diagenesis or grain size effects, as evidenced by the correlation between the C/N ratio and Mz of 0.42, $p = 0.03$. Consequently, marine sources were the dominant contributors to the core's organic carbon content.

The TOC content is intricately linked to primary productivity in the marine environment. Enhanced primary productivity is often correlated with an increase in the TOC content (Island, 2001; Khim et al., 2004; Mendonça et al., 2017). In high-latitude regions, the primary productivity exhibits notable seasonal and spatial variations and is primarily governed by light availability and climatic fluctuations. Consequently, the TOC content is a potential indicator of environmental change, reflecting alterations in the underlying productivity dynamics.

4.2 Tracing paleoenvironmental dynamics and underlying mechanisms in the Amundsen Sea since the mid-Holocene

Previous studies in the Ross Sea (Yongbin et al., 2021) and the Amundsen Sea (Hillenbrand et al., 2009) have established that the

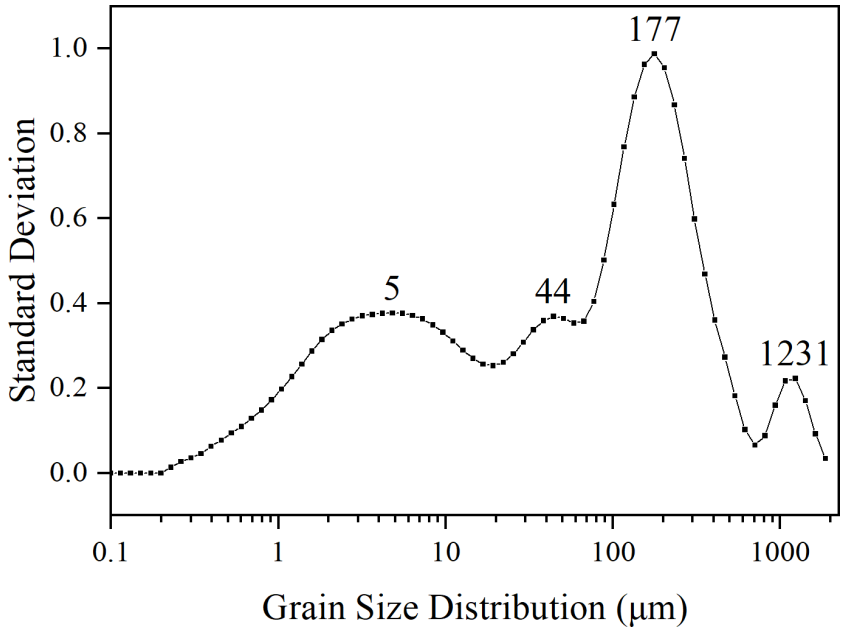

FIGURE 7
Grain size-standard deviation diagram of sediment in core ANT36-A11-04.

IRD variation was closely linked to environmental changes, making IRD a key indicator of glacial activity in the West Antarctic region. In high-latitude regions, the > 150 μm grain-size fraction in sediments is commonly used as a proxy for IRD. Our analysis of core ANT36-A11-04 (Figure 7) indicates that the 67–707 μm grain size interval was the most sensitive to environmental changes, with a pronounced peak at 177 μm. Thus, the > 150 μm fraction was selected as the IRD proxy in this study.

Through integration of multiple proxies, including the Cd/P ratio (indicative of CDW intensity) (Xu et al., 2021), $\delta^{13}C_{org}$ of organic matter and TOC content for core ANT36-A11-04, and the > 150 μm grain size (IRD proxy), we reconstructed the paleoenvironmental history of the Amundsen Sea. Spanning over 6,000 years, the core recorded six distinct environmental events (I–VI; Figure 8). Generally, the TOC and IRD trends corresponded with the variations in the intensity of the CDW. During 6000–3000 cal yr B.P, the TOC, IRD, and CDW decreased from the highest points to the average states. This pattern suggests a strong interconnection between the TOC, IRD, and CDW, that is, both the TOC and IRD decreased as the intensity of the CDW decreased, underscoring the influence of the CDW on these parameters. Additionally, there were noticeable peaks in both the TOC and IRD during the six periods studied. This trend was inversely reflected in the $\delta^{13}C_{org}$ record, suggesting that the $\delta^{13}C_{org}$ variations were associated with the TOC and IRD variations, and the CDW was also a potential influencing factor.

Our environmental evolution model (Figure 9) proposes that the upwelling of the relatively warm CDW contributed to accelerated glacier melting, enhancing sea ice melting and the subsequent release of IRD. The melting of sea ice facilitated a rapid exchange between the ocean and the atmosphere, leading to a marked negative shift in the $\delta^{13}C_{org}$ value of the marine plankton (Rau et al., 1989; Yager et al., 2016). Additionally, the influx of heat and nutrients associated with the CDW likely stimulated phytoplankton blooms, contributing to an increase in the TOC.

During event I (5800–5500 cal yr B.P), as illustrated in Figure 8, there was a concurrent peak in the TOC, and the > 150 μm particle size content coincided with a low $\delta^{13}C_{org}$ value. This pattern is indicative of an increased supply of IRD, potentially linked to intensified sea ice melting (Sakamoto et al., 2005). This period corresponded with a documented reduction in the sea ice content in the Weddell Sea, as evidenced by the abundance of foraminifera *F. curta* (Mezgec et al., 2017). A subsequent decline in the Cd/P ratio pointed to weakening of the intensity of the CDW, which likely led to diminished heat transfer to the sea surface. This reduction in heat transfer could have resulted in decreased ice shelf melting or augmented sea ice coverage (Thoma et al., 2008; Guo et al., 2019). Consequently, this led to a decrease in the supply of IRD and lower availability of light and nutrients, which in turn resulted in a decrease in the TOC. The observed decrease in the $\delta^{13}C_{org}$ value was influenced by multiple factors (Rau et al., 1989; Goericke and Fry, 1994; Annett et al., 2007). When phytoplankton absorb carbon from the inorganic carbon pool, they are more inclined to absorb lighter isotopes at higher inorganic carbon concentrations (Mook et al., 1974). These factors were linked to the changes in the CDW, as a decline in the intensity of the CDW resulted in decreased heat and nutrient transport to the sea surface (Fei et al., 2019; Xu et al., 2021).

The subsequent events, II (5100–4600 cal yr B.P), III (3900–3200 cal yr B.P), IV (2600–2000 cal yr B.P), V (1800–1300 cal yr B.P), and VI (1100–500 cal yr B.P), exhibited similar patterns. The IRD and TOC exhibited opposite patterns compared to that of the $\delta^{13}C_{org}$. The presence of an IRD deposition pattern was evident in the sediment in core ANT36-A11-04, which is consistent with the ice retreat-associated IRD input events in the Ross Sea and the Amundsen Sea (Hillenbrand et al., 2009; Yongbin et al., 2021). This pattern can be

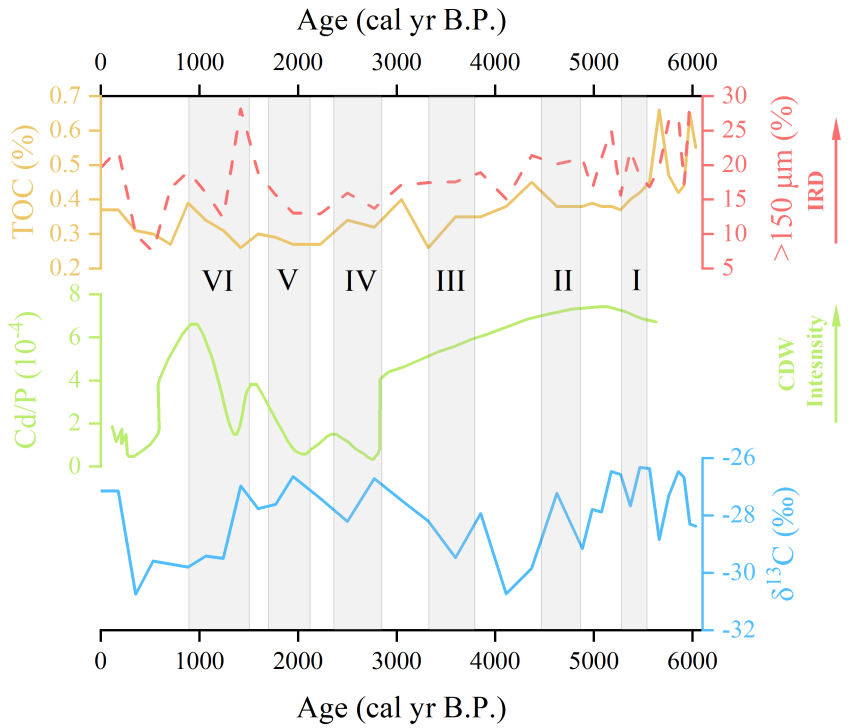

FIGURE 8
The response relationship between $\delta^{13}C_{org}$ and the environment and its potential mechanism. The yellow solid line denotes the TOC content in core ANT36-A11-04, the red dashed line indicates the > 150 μm fraction content in the core, the green solid line denotes the Cd/P ratio within the penguin ornithogenic sediments from the Ross Sea, which indicates the intensity of the CDW (Xu et al., 2021), and the blue solid line denotes the $\delta^{13}C_{org}$ of the organic matter within the core sediments.

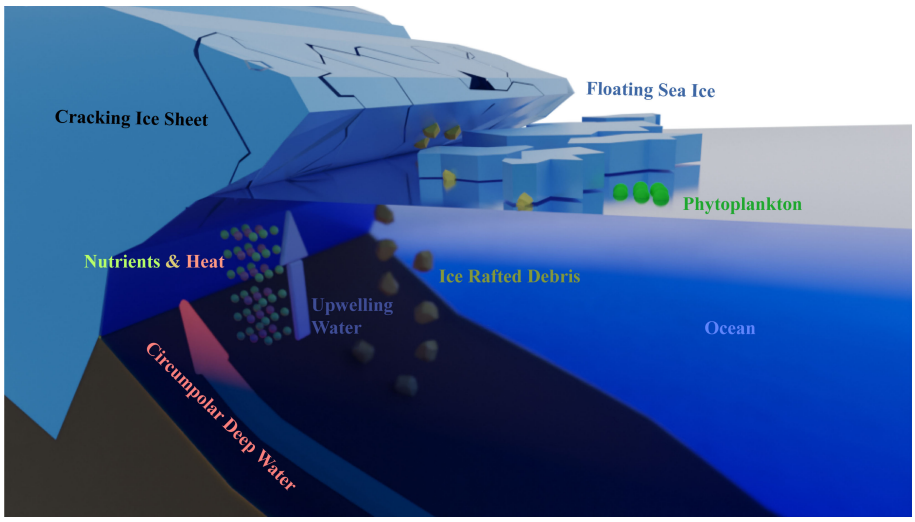

FIGURE 9
Environmental evolution pattern. The Circumpolar Deep Water (CDW) (depicted in red) intruded beneath the ice shelf (depicted as a blue opaque polyhedron with cracking details). The upwelling CDW is shown as upwelling water (indicated by the dark blue arrow), which carries both nutrients (shown as small green spheres) and heat (shown as red spheres) toward the sea surface. This upwelling fostered the proliferation of phytoplankton (illustrated as larger green spheres) near the floating sea ice. Additionally, this process contributed to the melting of the ice shelf and sea ice, leading to the release of ice-rafted debris (yellow and brown particles), which then became incorporated into the ocean sediments.

attributed to the influence of the upwelling of warm CDW on the ice shelves in the Amundsen Sea sector. As the grounding line of the ice shelves retreated, significant amounts of land-derived detritus were unloaded, leading to IRD deposition events and the formation of glacial debris deposits on the continental shelf (Anderson et al., 2014). When the heat flux decreased and the sea ice coverage expanded, the melting of icebergs slowed, resulting in decreased IRD deposition, reduced primary production, and a lower TOC.

Our analysis of the sediment in core ANT36-A11-04 suggests that the CDW profoundly impacted the local environmental changes, including the sea ice dynamics, blooming of phytoplankton, and IRD deposition (Figure 9). The core record illustrates that the close association between the CDW, $\delta^{13}C_{org}$, and IRD values suggests that the CDW played a critical role in the regional environmental evolution process. The reduction in the intensity of the CDW resulted in a decreased water temperature, reduced ice shelf melting, diminished IRD input, and a reduced production rate of organically derived phytoplankton. In summary, the existence of this coupled model emphasizes the importance of the CDW in the environmental changes in the Amundsen Sea region.

5 Conclusions

Over the past decade, many researchers have found that the atmosphere and ocean currents in West Antarctic played a key role in the environmental evolution in this region. In particular, the CDW deeply influenced the glaciers and ecosystem. To determine the relationship between the CDW and the environmental changes, several analyses were performed in this study. The three main conclusions are presented below.

1. By examining the sediment of core ANT36-A11-04 and integrating prior research findings, it was found that the primary source of the organic matter in the sediment was largely oceanic.
2. The > 150 μm grain size component in core ANT36-A11-04 was utilized as an alternative indicator of IRD, in combination with other indicators such as $\delta^{13}C_{org}$, TOC, and proxy for the CDW. Through these indicators, six environmental events were identified, each with corresponding records in the Antarctic region.
3. By comparing multiple indicators, it was observed that there was a clear response relationship between the $\delta^{13}C_{org}$, IRD, and CDW, indicating that the CDW played a critical role in the regional environmental evolution. The upwelling of the relatively warm CDW led to accelerated glacier melting and increased heat flux, which also enhanced the melting of sea ice. This process resulted in the release and deposition of IRD carried by glacial and sea ice. Furthermore, the heat and nutrients transported by the upwelling water stimulated the proliferation of marine plankton. Additionally, the melting of sea ice enhanced the rapid exchange between the ocean and the atmosphere, ultimately causing a noticeable negative shift in the $\delta^{13}C_{org}$ value of the marine plankton.

Data availability statement

The raw data supporting the conclusions of this article will be made available by the authors, without undue reservation.

Author contributions

ZL: Software, Visualization, Writing – original draft, Writing – review & editing. QG: Funding acquisition, Methodology, Resources, Supervision, Writing – review & editing. DC: Investigation, Validation, Writing – review & editing. YZ: Investigation, Resources, Software, Writing – review & editing. XH: Investigation, Methodology, Resources, Writing – review & editing.

Funding

The author(s) declare financial support was received for the research, authorship, and/or publication of this article. This work was funded by the Impact and Response of Antarctic Seas to Climate Change (IRASCC). This project provided us with cruise and funding for sampling and analysis.

Acknowledgments

Supported by the crew and researchers of the 36th Chinese Antarctic Research Expedition, and it was reviewed by reviewers and editors. We thank them for their patience and time.

Conflict of interest

The authors declare that the research was conducted in the absence of any commercial or financial relationships that could be construed as a potential conflict of interest.

Publisher's note

Supplementary material

The Supplementary Material for this article can be found online at: https://www.frontiersin.org/articles/10.3389/fmars.2023.1284750/full#supplementary-material

References

Albuquerque, A. L. S., and Mozeto, A. A. (1997). C: N: P ratios and stable carbon isotope compositions as indicators of organic matter sources in a riverine wetland system (Moji-guaçu River, São Paulo-Brazil). *Wetlands* 17, 1–9. doi: 10.1007/BF03160713

Anderson, J. B., Conway, H., Bart, P. J., Witus, A. E., Greenwood, S. L., McKay, R. M., et al. (2014). Ross Sea paleo-ice sheet drainage and deglacial history during and since the LGM. *Quat. Sci. Rev.* 100, 31–54. doi: 10.1016/j.quascirev.2013.08.020

Annett, A. L., Carson, D. S., Ganeshram, R. S., and Fallick, A. E. (2007). "Ecological influences on δ13C of particulate matter in seasonally ice-covered Ryder Bay." *Antarctica–Online Proceedings of the 10th ISAES X* edited by A. K. Cooper, C. R. Raymond, et al. USGS Open-File Report 1047 (2007).

Delmont, T. O., Hammar, K. M., Ducklow, H. W., Yager, P. L., and Post, A. F. (2014). Phaeocystis Antarctica blooms strongly influence bacterial community structures in the Amundsen Sea polynya. *Front. Microbiol.* 5. doi: 10.3389/fmicb.2014.00646

Domack, E. W., Jacobson, E. A., Shipp, S., and Anderson, J. B. (1999). Late Pleistocene–Holocene retreat of the West Antarctic Ice-Sheet system in the Ross Sea: Part 2—Sedimentologic and stratigraphic signature. *GSA Bull.* 111, 1517–1536. doi: 10.1130/0016-7606(1999)111<1517:LPHROT>2.3.CO;2

Ducklow, H. W., Wilson, S. E., Post, A. F., Stammerjohn, S. E., Erickson, M., Lee, S., et al. (2015). Particle flux on the continental shelf in the Amundsen Sea Polynya and Western Antarctic PeninsulaAntarctic particle flux. *Elem. Sci. Anthr* 3, 000046. doi: 10.12952/journal.elementa.000046

Fei, X., Zhang, Z., Cheng, Z., and Santosh, M. (2019). Factors controlling the crystal morphology and chemistry of garnet in skarn deposits: A case study from the Cuihongshan polymetallic deposit, Lesser Xing'an Range, NE China. *Am. Mineral.* 104, 1455–1468. doi: 10.2138/am-2019-6968

Goericke, R., and Fry, B. (1994). Variations of marine plankton δ13C with latitude, temperature, and dissolved CO2 in the world ocean. *Glob. Biogeochem. Cycles* 8, 85–90. doi: 10.1029/93GB03272

Gudmundsson, G. H., Paolo, F. S., Adusumilli, S., and Fricker, H. A. (2019). Instantaneous Antarctic ice sheet mass loss driven by thinning ice shelves. *Geophys. Res. Lett.* 46, 13903–13909. doi: 10.1029/2019GL085027

Guo, G., Shi, J., Gao, L., Tamura, T., and Williams, G. D. (2019). Reduced sea ice production due to upwelled oceanic heat flux in Prydz Bay, East Antarctica. *Geophys. Res. Lett.* 46, 4782–4789. doi: 10.1029/2018GL081463

Heroy, D. C., and Anderson, J. B. (2007). Radiocarbon constraints on Antarctic Peninsula ice sheet retreat following the Last Glacial Maximum (LGM). *Quat. Sci. Rev.* 26, 3286–3297. doi: 10.1016/j.quascirev.2007.07.012

Hillenbrand, C.-D., Kuhn, G., and Frederichs, T. (2009). Record of a Mid-Pleistocene depositional anomaly in West Antarctic continental margin sediments: an indicator for ice-sheet collapse? *Quat. Sci. Rev.* 28, 1147–1159. doi: 10.1016/j.quascirev.2008.12.010

Hillenbrand, C.-D., Smith, J. A., Kuhn, G., Esper, O., Gersonde, R., Larter, R. D., et al. (2010). Age assignment of a diatomaceous ooze deposited in the western Amundsen Sea Embayment after the Last Glacial Maximum. *J. Quat. Sci.* 25, 280–295. doi: 10.1002/jqs.1308

Island, G. (2001). South Shetland islands. *Antarct. Sci.* 7, 99–113.

Jenkins, A., Dutrieux, P., Jacobs, S. S., McPhail, S. D., Perrett, J. R., Webb, A. T., et al. (2010). Observations beneath Pine Island Glacier in West Antarctica and implications for its retreat. *Nat. Geosci.* 3, 468–472. doi: 10.1038/ngeo890

Joughin, I., and Alley, R. B. (2011). Stability of the West Antarctic ice sheet in a warming world. *Nat. Geosci.* 4, 506–513. doi: 10.1038/ngeo1194

Anderson, J., and Andrew, J. (1999). Radiocarbon constraints on ice sheet advance and retreat in the Weddell Sea, Antarctica. *Geology* 27 (2), 179–182. doi: 10.1130/0091-7613(1999)027<0179:RCOISA>2.3.CO;2

Khim, B.-K., Yoon, H.-I., Kang, C.-Y., and Zhao, J. (2004). Holocene variations of organic carbon contents in lake Langer of king George island, South Shetland islands, West Antarctica. *Ocean Polar Res.* 26, 507–514. doi: 10.4217/OPR.2004.26.3.507

Licht, K. J., and Andrews, J. T. (2002). The 14C record of late pleistocene ice advance and retreat in the central ross sea, Antarctica. *Arct. Antarct. Alp. Res.* 34, 324–333. doi: 10.1080/15230430.2002.12003501

Licht, K. J., and Hemming, S. R. (2017). Analysis of Antarctic glacigenic sediment provenance through geochemical and petrologic applications. *Quat. Sci. Rev.* 164, 1–24. doi: 10.1016/j.quascirev.2017.03.009

Licht, K.J., Jennings, A.E., Andrews, J.T., and Williams, K.M. (1996). Chronology of late Wisconsin ice retreat from the western Ross Sea Antarctica. *Geology* 24, 223–226.

Liu, S., LI, J., Fang, X., Zhang, H., Yu, Y., Cao, P., et al. (2007). National Standards of People's Republic of China: Specifications for oceanographic survey - Part 8: Marine geology and geophysics survey. *Beijing, China, China Standards Press for China National Standardization Administration*, 139pp. doi: 10.25607/OBP-151

Lowe, A. L., and Anderson, J. B. (2002). Reconstruction of the West Antarctic ice sheet in Pine Island Bay during the Last Glacial Maximum and its subsequent retreat history. *Quat. Sci. Rev.* 21, 1879–1897. doi: 10.1016/S0277-3791(02)00006-9

Lupton, J.E., and Craig, H. (1981). A major helium-3 source at 15°S on the East Pacific Rise. *Science* 214, 13-18. doi: 10.1126/science.214.4516.13

Mallett, H. K., Boehme, L., Fedak, M., Heywood, K. J., Stevens, D. P., and Roquet, F. (2018). Variation in the distribution and properties of Circumpolar Deep Water in the eastern Amundsen Sea, on seasonal timescales, using seal-borne tags. *Geophys. Res. Lett.* 45, 4982–4990. doi: 10.1029/2018GL077430

Mendonça, R., Müller, R. A., Clow, D., Verpoorter, C., Raymond, P., Tranvik, L. J., et al. (2017). Organic carbon burial in global lakes and reservoirs. *Nat. Commun.* 8, 1694. doi: 10.1038/s41467-017-01789-6

Mezgec, K., Stenni, B., Crosta, X., Masson-Delmotte, V., Baroni, C., Braida, M., et al. (2017). Holocene sea ice variability driven by wind and polynya efficiency in the Ross Sea. *Nat Commun* 8, 1334. doi: 10.1038/s41467-017-01455-x

Minoura, K., Hoshino, K., Nakamura, T., and Wada, E. (1997). Late Pleistocene-Holocene paleoproductivity circulation in the Japan Sea: sea-level control on δ13C and δ15N records of sediment organic material. *Palaeogeogr. Palaeoclimatol. Palaeoecol.* 135, 41–50. doi: 10.1016/S0031-0182(97)00026-6

Mook, W. G., Bommerson, J. C., and Staverman, W. H. (1974). Carbon isotope fractionation between dissolved bicarbonate and gaseous carbon dioxide. *Earth Planet. Sci. Lett.* 22, 169–176. doi: 10.1016/0012-821X(74)90078-8

Mosola, A. B., and Anderson, J. B. (2006). Expansion and rapid retreat of the West Antarctic Ice Sheet in eastern Ross Sea: possible consequence of over-extended ice streams? *Quat. Sci. Rev.* 25, 2177–2196. doi: 10.1016/j.quascirev.2005.12.013

Nakayama, Y., Menemenlis, D., Zhang, H., Schodlok, M., and Rignot, E. (2018). Origin of Circumpolar Deep Water intruding onto the Amundsen and Bellingshausen Sea continental shelves. *Nat. Commun.* 9, 3403. doi: 10.1038/s41467-018-05813-1

Nakayama, Y., Schröder, M., and Hellmer, H. H. (2013). From circumpolar deep water to the glacial meltwater plume on the eastern Amundsen Shelf. *Deep Sea Res. Part Oceanogr. Res. Pap.* 77, 50–62. doi: 10.1016/j.dsr.2013.04.001

Nakayama, Y., Timmermann, R., Schröder, M., and Hellmer, H. H. (2014). On the difficulty of modeling Circumpolar Deep Water intrusions onto the Amundsen Sea continental shelf. *Ocean Model.* 84, 26–34. doi: 10.1016/j.ocemod.2014.09.007

Naughten, K. A., Holland, P. R., and De Rydt, J. (2023). Unavoidable future increase in West Antarctic ice-shelf melting over the twenty-first century. *Nat. Clim. Change* 13, 1222–1228. doi: 10.1038/s41558-023-01818-x

Nicolas, J. P., and Bromwich, D. H. (2011). Climate of West Antarctica and influence of marine air intrusions. *J. Clim.* 24, 49–67. doi: 10.1175/2010JCLI3522.1

Ohkouchi, N., and Eglinton, T. I. (2006). Radiocarbon constraint on relict organic carbon contributions to Ross Sea sediments. *Geochem. Geophys. Geosyst.* 7, Q04012. doi: 10.1029/2005GC001097

Rau, G. H., Takahashi, T., and Marais, D. J. D. (1989). Latitudinal variations in plankton δ13C: implications for CO2 and productivity in past oceans. *Nature* 341, 516–518. doi: 10.1038/341516a0

Sakamoto, T., Ikehara, M., Aoki, K., Iijima, K., Kimura, N., Nakatsuka, T., et al. (2005). Ice-rafted debris (IRD)-based sea-ice expansion events during the past 100 kyrs in the Okhotsk Sea. *Deep Sea Res. Part II Top. Stud. Oceanogr.* 52, 2275–2301. doi: 10.1016/j.dsr2.2005.08.007

Shultz, D. J., and Calder, J. A. (1976). Organic carbon 13C12C variations in estuarine sediments. *Geochim. Cosmochim. Acta* 40, 381–385. doi: 10.1016/0016-7037(76)90002-8

Smith, J. A., Hillenbrand, C.-D., Kuhn, G., Klages, J. P., Graham, A. G. C., Larter, R. D., et al. (2014). New constraints on the timing of West Antarctic Ice Sheet retreat in the eastern Amundsen Sea since the Last Glacial Maximum. *Glob. Planet. Change* 122, 224–237. doi: 10.1016/j.gloplacha.2014.07.015

Smith, J. A., Hillenbrand, C.-D., Kuhn, G., Larter, R. D., Graham, A. G., Ehrmann, W., et al. (2011). Deglacial history of the West Antarctic Ice Sheet in the western Amundsen Sea embayment. *Quat. Sci. Rev.* 30, 488–505. doi: 10.1016/j.quascirev.2010.11.020

Spezie, G. (1999). *Oceanography of the ross sea: Antarctica* (Springer).

Stein, R., and Fahl, K. (2000). Holocene accumulation of organic carbon at the Laptev Sea continental margin (Arctic Ocean): sources, pathways, and sinks. *Geo-Mar. Lett.* 20, 27–36. doi: 10.1007/s003670000028

Stuiver, M., and Reimer, P. J. (1993). Extended 14C data base and revised CALIB 3.0 14C age calibration program. *Radiocarbon* 35, 215–230. doi: 10.1017/S0033822200013904

Thoma, M., Jenkins, A., Holland, D., and Jacobs, S. (2008). Modelling circumpolar deep water intrusions on the Amundsen Sea continental shelf, Antarctica. *Geophys. Res. Lett.* 35. doi: 10.1029/2008GL034939

van Manen, M., Aoki, S., Brussaard, C. P. D., Conway, T. M., Eich, C., Gerringa, L. J. A., et al. (2022). The role of the Dotson Ice Shelf and Circumpolar Deep Water as driver and source of dissolved and particulate iron and manganese in the Amundsen Sea polynya, Southern Ocean. *Mar. Chem.* 246, 104161. doi: 10.1016/j.marchem.2022.104161

Xu, Q. B., Yang, L. J., Gao, Y. S., Sun, L. G., and Xie, Z. Q. (2021). 6,000-year reconstruction of modified circumpolar deep water intrusion and its effects on sea ice and penguin in the ross sea. *Geophys. Res. Lett.* 48, e2021GL094545. doi: 10.1029/2021GL094545

Yager, P., Sherrell, R., Stammerjohn, S., Ducklow, H., Schofield, O., Ingall, E., et al. (2016). A carbon budget for the Amundsen Sea Polynya, Antarctica: Estimating net community production and export in a highly productive polar ecosystem. *Elem. Sci. Anthr.* 4, 140. doi: 10.12952/journal.elementa.000140

Yongbin, L., Rujian, W., Li, W. U., and Wenshen, X. (2021). Glacial dynamics evolutions revealed by ice-rafted detritus record from the Ross Sea sector of the Southern Ocean since Late Pleistocene. *Quat. Sci.* 41, 662–677. doi: 10.11928/j.issn.1001-7410.2021.03.04